Crop inventory at regional scale in Ukraine: developing in season and end of season crop maps with multi-temporal optical and SAR satellite imagery

Nataliia Kussul, Lavreniuk Mykola, Andrii Shelestov & Sergii Skakun

Published online: 29 May 2018.

Submit your article to this journal

View related articles

View Crossmark data

Taylor & Francis
Taylor & Francis Group

Crop inventory at regional scale in Ukraine: developing in season and end of season crop maps with multi-temporal optical and SAR satellite imagery

Nataliia Kussul [a,b], Lavreniuk Mykola [a,b], Andrii Shelestov [a,b] and Sergii Skakun [c,d]

aDepartment of Space Information Technologies and Systems, Space Research Institute NAS Ukraine & SSA Ukraine, Kyiv, Ukraine;
bDepartment of Information Security, National Technical University of Ukraine "Igor Sikorsky Kyiv Polytechnic Institute", Kyiv, Ukraine;
cDepartment of Geographical Sciences, University of Maryland, College Park, MD, USA; dNASA Goddard Space Flight Center (GSFC) Terrestrial Information Systems Laboratory Code 619, Greenbelt, MD, USA

ABSTRACT

Along the season crop classification maps based on satellite data is a challenging task for countries with large diversity of agricultural crops with different phenology (crop calendars). In this paper, we investigate feasibility of delivering early and along the season crop specific maps using available free satellite data over multiple years, including Landsat-8, Sentinel-1 and Sentinel-2. For this study, a test site in Kyiv region (Ukraine) is selected, for which we have been collecting ground data on crop types every year since 2011. Crop type maps are generated through a supervised classification of multi-temporal multi-source satellite data using previously developed artificial neural network algorithms. It is shown, how multi-year crop classification maps are used for crop rotation violation detection. The study shows that in case of considerable cloud cover, synthetic aperture radar (SAR) data, for example acquired by Sentinel-1 satellite, can be interchangeably used with optical imagery to achieve the target 85% accuracy for crop classification.

Introduction

Crop mapping with remote sensing data

Availability of reliable and accurate crop maps at regional and national scale is a prerequisite for efficient monitoring of agricultural land use. A wide range of agricultural applications, including crop area estimation, crop yield forecasting, crop state assessment, land use intensity rely heavily on the use of crop maps. Information on crop frequency derived from historical maps can be effectively used for stratification purposes in crop area estimation (Boryan, Yang, Di, & Hunt, 2014; Gallego et al., 2012). Knowing geographical distribution of given crops can help optimize available resources, when performing large scale ground observations (Song et al., 2017). For instance, early season crop masks are required to provide crop yield prediction and, consequently, crop production forecasting in the operational context which is important for food security (Becker-Reshef, Vermote, Lindeman, & Justice, 2010; Franch et al., 2015; Johnson, 2016; Kogan et al., 2013; López-Lozano et al., 2015; Shao, Campbell, Taff, & Zheng, 2015). Crop maps can be incorporated into the drought risk assessment models to quantify and map the risk at different scales (Skakun, Kussul, Shelestov, & Kussul, 2016a). Availability of multi-year crop maps can be used to estimate land use intensity, which includes crop planting frequency and crop

rotation (Kuemmerle et al., 2013). Also, time-series of such maps is essential for detection of crop rotation violations, which usually lead to soil degradation and decrease of crop production.

Earth observation (EO) remain one of the most important data sources for developing crop maps and crop inventories (Cohen & Goward, 2004). This is mainly due to capabilities to timely acquire images in different spectral bands and provide repeatable, continuous, human independent measurements for large territories. In particular, optical instruments onboard remote-sensing satellites provide imagery in multiple spectral bands, usually in visible, near-infrared, short wave infrared, and thermal infrared. However, these data can be contaminated with cloud cover that, in many cases, makes it very difficult to acquire imagery in an optimal time range to discriminate crops (Pax-Lenney & Woodcock, 1997; Prishchepov, Radeloff, Dubinin, & Alcantara, 2012). On the other hand, synthetic aperture radar (SAR) instruments offer unique features to image crops due to their all-weather capabilities and ability to capture crop characteristics different from those derived from optical instruments (Skakun, Kussul, Shelestov, Lavreniuk, & Kussul, 2016b; Stefanski, Chaskovskyy, & Waske, 2014). Thanks to this,

CONTACT Lavreniuk Mykola ✉ nick_93@ukr.net 🖳 Department of Space Information Technologies and Systems, Space Research Institute NAS Ukraine & SSA Ukraine, Glushkov Prospekt 40, Kyiv 03680, Ukraine

SAR imagery can be captured at the best suited dates.

To this end, several programmes exist that target the development of crop inventories utilizing EO data, both optical and radar. The creation of the Cropland Data Layer (CDL) of the US Department of Agriculture (USDA) National Agricultural Statistics Service (NASS) is considered as one of the most successful applications of remote sensing data for crop mapping at national scale (Boryan, Yang, Mueller, & Craig, 2011; Johnson & Mueller, 2010). The CDL product provides crop maps for 47 states at 56 m spatial resolution from 2008 until 2010 and at 30 m spatial resolution after 2010. The primary source of remote sensing images is Advanced Wide Field Sensor (AWiFS), Deimos-1, Landsat-5/7/8, UK Disaster Monitoring Constellation (UK-DMC) and Moderate Resolution Imaging Spectroradiometer (MODIS). Supervised classification based on the classification and regression tree (CART) decision trees (DTs) is used to classify multi-temporal images into 25 crop-specific classes with accuracies for 2009 ranging from 85% to 95% for the major crops (corn, soybeans, and winter wheat). To train the classifier for satellite image classification, administrative data from Farm Service Agency-Common Land Units (FSA-CLU) are used. For crop area estimation, however, the main source of information is the June Area Survey (JAS) in which approximately 11,000, 1 sq mi sample segments are visited by enumerators to collect crop type and acreage information (Boryan et al., 2014). These JAS data provide the main variable for the regression estimator in crop area estimation. In general, CDL is used to drive the sampling strategies within the JAS surveys, and a key component for crop yield modelling (Johnson & Mueller, 2010). Agriculture and Agri-Food Canada (AAFC) provides the Annual Crop Inventory product, which is developed using optical (Landsat-5, AWiFS, DMC) and SAR (Radarsat-2) images. Multi-temporal satellite images are classified using the DT (CART) approach enabling the overall target accuracy of at least 85%. The product is delivered at 30 m spatial resolution (56 m in 2009–2010) (AAFC, 2013). The main source of ground truth data for training and validation of the product is annual crop insurance data derived from farmers. In Europe, regional crop inventories (Taylor, Sannier, Delince, & Gallego, 1997) utilized the USDA approach with area frame samples as main variable and classified satellite imagery as a co-variable. Attempts to produce rapid estimates of inter-annual crop area for the European Union (EU) using images without current field data showed that the results had depended more on the a priori belief of the analyst than on the information provided by the images (Gallego, 2006). Currently, the main usage of remote sensing imagery in the EU within the Land Use and Cover Area-Frame Statistical Survey (LUCAS) lies in stratification, while ground surveys remain the main source of information for land cover and crop area estimation (Gallego & Delincé, 2010).

Objective of the study

Ukraine is one of the most developed agricultural countries in the world. According to the U.S. Department of Agriculture (USDA) Foreign Agricultural Service (FAS) statistics, Ukraine was the largest sunflower producer (11.6 MT) and exporter, and the ninth largest wheat producer (22.2 MT) in the world in 2013. Providing multi-annual crop inventory is extremely important for managing agricultural resources at regional and national scale in Ukraine. A Joint Experiment for Crop Assessment and Monitoring (JECAM) test site was established in Ukraine in 2011 with the aim to develop and validate different methodologies for monitoring agricultural resources with the help of remote sensing data (Kussul et al., 2016; Skakun et al., 2016b). These include techniques for delivering in season and end of season crop maps by classifying multi-temporal optical and SAR satellite imagery. In this paper, we aim at creating a crop inventory for multiple seasons at regional scale in Ukraine using multi-temporal remote sensing images to provide similar maps available for USA and Canada. Direct application of the US or Canada-based approaches for Ukraine is difficult because of unavailability of data from farmers that leads to exploiting other sampling strategies, e.g. collecting data along the roads (Waldner et al., 2016). The similarity lies in using all freely available satellite imagery, both optical and SAR, and exploiting different machine learning algorithms such as random forest and neural networks (Kussul, Lavreniuk, Skakun, & Shelestov, 2017). The maps, both in season and end of season, are produced utilizing all available moderate spatial resolution satellite data, namely 30 m Landsat-8 Operational Land Imager (OLI) (2013–2015), 10 m Sentinel-1A C-band SAR (2015–2016), and 10 m Sentinel-2 Multi-Spectral Instrument (MSI) (2016). A machine learning technique based on ensemble of artificial neural networks (multi-layer perceptrons – MLPs) (Kussul et al., 2015) is used to classify satellite images into major crop types for 2013–2015 seasons. An application of using these maps for crop rotation violation detection is considered as well.

Study area and materials description

The experimental site

One administrative districts (Bilotserkivskiy) in Kyiv region has been selected for this study (Figure 1).
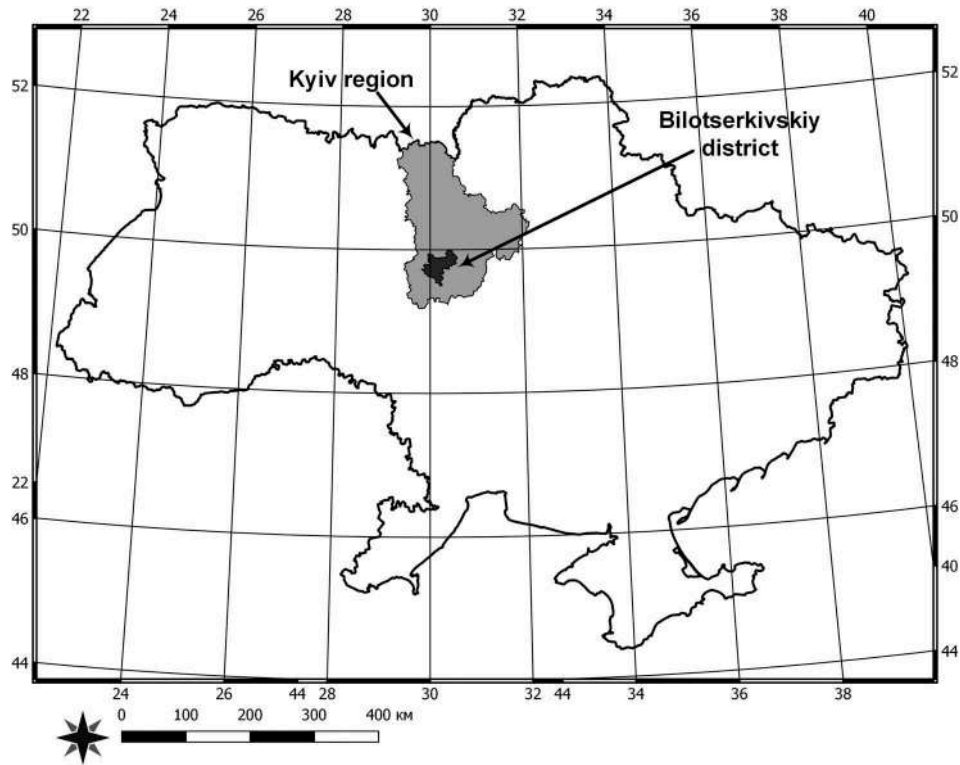
Figure 1. Study area: Bilotserkivskiy district in Kyiv region.

Kyiv region with geographic area of 28,100 km² and almost 1.0M ha of cropland is located in the north-central part of Ukraine. The area of Bilotserkivskiy district is 1,276 km². Soybeans, maize, winter wheat, sunflower, spring wheat and spring barley are the main crops in this region with major non-crop classes being grassland, forest and water. Our test site is located not far from the Dnipro river, and in general vegetation period is September–July for winter crops, and April–October for spring and summer crops.

Satellite data

For this study, we used 10 m SAR and optical satellite data from the Sentinel-1A and Sentinel-2 with the revisit time 12 and 10 days, respectively (Figure 2). Level-1 Interferometric Wide mode Ground Range Detected (IW-GRD) Sentinel-1A products in VV and VH polarizations have been used. All Sentinel-1A images were processed using the Sentinel-1 Toolbox (S1TBX) 1.0.3. Images were multi-looked with a 2 × 2 window, and filtered using a single product Refined Lee filter with a 3 × 3 window to reduce speckle level (Moreira et al., 2013). SAR images were further geometrically corrected using a Range-Doppler terrain correction procedure with the SRTM 3Sec Digital Elevation Model (DEM). The last step of SAR images pre-processing involved calibration to a backscatter coefficient (Moreira et al., 2013). In the experiment with the fusion of Sentinel-1 and Landsat-8 data, we re-sampled SAR images to Landsat-8 spatial resolution at 30 m. Multi-spectral high-resolution optical observations were provided by Sentinel-2. Level-1C top of atmosphere (TOA) reflectance product that consists of 100 × 100 km² tiles was used for crop mapping. We considered three

Figure 2. An example of Sentinel-2 true colour composite (08.04.2016) for Bilotserkivskiy district (a), Sentinel-1A (12.04.2016) image (VV and VH polarizations) for Bilotserkivskiy district (b).

Table 1. Landsat-8, Sentinel-1A and Sentinel-2 data availability for the Bilotserkivskiy district in 2013–2016.

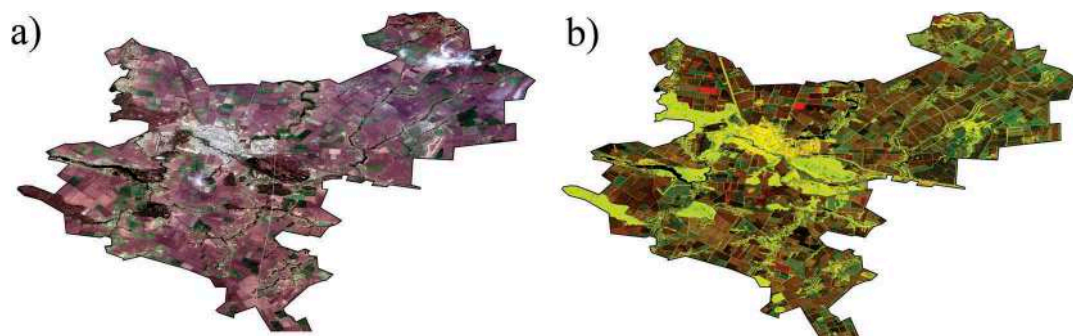| Year	Landsat-8	Sentinel-1A	Sentinel-2
2016	–	07.03, 19.03, 31.03, 12.04, 24.04, 06.05, 18.05, 30.05	08.04, 28.04
2015	24.05, 9.06, 25.06, 28.08	01.03, 13.03, 25.03, 06.04, 18.04, 30.04, 12.05, 24.05, 05.06, 17.06, 29.06, 11.07, 23.07, 16.08, 28.08	–
2014	03.04, 06.06, 08.07, 10.09, 12.10, 28.10	–	–
2013	16.04, 02.05, 18.05, 19.06, 05.07, 06.08	–	–

visible bands (red, green, blue) and near-infrared band which all have 10 m spatial resolution. For the Bilotserkivskiy district in Kyiv region in 2013 Landsat-8 satellite images were pre-processed to remove the effect of atmosphere using the Simplified Model for Atmospheric Correction (SMAC) (Rahman & Dedieu, 1994). Therefore, each pixel value was converted to the surface reflectance (SR) value; for 2014–2015 we used only top of atmosphere (TOA) reflectance values (Table 1). Multi-temporal Landsat-8 OLI 2–7 bands were reconstructed using self-organizing maps (SOMs) to restore missing reflectance values due to clouds and shadows (Kussul et al., 2017), and used for classification of satellite imagery. Landsat-8 bands 1 and 9 were not used due to the strong atmospheric influence. The panchromatic band and thermal bands from the Thermal Infrared Sensor (TIRS) were not utilized either.

We used SAR scenes from the 36th and 007th relative orbit numbers, Landsat-8 images with 181/ 25 path/row coordinate and Sentinel-2 data with 36TVT and 35UQR tiles (https://sentinel.esa.int/web/sentinel/missions/sentinel-1/observation-scenario/acquisition-segments).

Ground reference data

Ground surveys for *insitu* data collection to support crop classification using satellite imagery were conducted in 2013–2016. The European Land Use and Cover Area frame Survey (LUCAS) nomenclature (Gallego & Delincé, 2010) was used in this study as a basis for land cover/land use types. For 2013–2015 years, we had 13 land cover classes, including the following crops: winter wheat, winter rapeseed, maize, sugar beet, sunflower, soybeans, other spring crops and other cereals (Table 2). For 2016, we had only 7 land cover classes: winter wheat, winter rapeseed, winter barley, spring and summer crops, forest, grassland and water (Table 3).

Methodology description

One of the main challenges in classification of multi-temporal optical satellite imagery is the presence of missing values caused by clouds and shadows. In previous works, we proposed an approach that combines unsupervised and supervised neural networks for missing data restoration and supervised classification, respectively (Kussul et al., 2015; Skakun et al., 2016b). First, self-organizing Kohonen maps (SOMs) are applied to restore missing pixel values in a time series of optical satellite imagery. However, with persistent cloud cover, especially during an early season, optical imagery is not enough to achieve the desirable accuracy of 85%. Therefore, SAR imagery is fused with optical ones to improve discrimination of crops when optical images are not available (Kussul et al., 2016; Skakun et al., 2016b). *In situ* samples have been randomly divided into two independent subsets: training set (50% of polygons for each class) and test set (50% of polygons for each class). Then, a supervised classification is performed to classify multi-temporal satellite images (Skakun, Nasuro, Lavrenyuk, & Kussul, 2007). For this, a committee of NNs, in particular multi-layer

Table 2. Number of polygons and total area of crops and land cover types collected during the ground surveys for the Bilotserkivskiy district in 2013–2015.

#	Class	2013		2014		2015	
		Fields	Area, ha	Fields	Area, ha	Fields	Area, ha
1	Artificial	6	23.0	15	53.0	0	0
2	Winter wheat	51	3960.8	125	7589.4	102	3695.9
3	Winter rapeseed	12	937.3	36	1686.6	22	715.9
4	Spring crops	9	455.9	44	1358.0	11	296.0
5	Maize	87	7253.3	76	4030.4	98	4329.1
6	Sugar beet	8	632.5	18	1624.5	8	860.7
7	Sunflower	30	2549.0	31	1338.2	53	1954.0
8	Soybeans	60	3252.3	108	2965.3	87	3006.9
9	Other cereals	32	1364.0	12	451.9	0	0
10	Forest	17	1014.3	35	1750.7	49	2012.3
11	Grassland	48	747.5	67	1528.8	64	952.3
12	Bare land	10	67.2	10	69.6	10	71.4
13	Water	16	448.3	31	578.9	43	1072.1
	Total	**386**	**22,705.3**	**608**	**25,025.3**	**547**	**18,966.6**

Table 3. Number of polygons and total area of crops and land cover types collected during the ground surveys for the Bilotserkivskiy district in 2016.

#	Class	Bilotserkivskiy	
		Fields	Area, ha
1	Winter wheat	117	4255
2	Winter barley	6	203
3	Winter rapeseed	15	454
4	Spring and summer crops	150	5611
5	Forest	44	1100
6	Grassland	32	250
7	Water	17	109
	Total	**381**	**11,982**

perceptrons (MLPs), is utilized to improve the performance of individual classifiers (Kussul et al., 2015). The MLP classifier has a hyperbolic tangent activation function for neurons in the hidden layer and logistic activation function in the output layer. The committee is formed using four MLPs with different number of hidden neurons (10, 20, 30, and 40) trained on the same training data within 250 epochs. Outputs from different MLPs are integrated using the technique of average committee. Under this technique, the average class probability over classifiers is calculated, and the class with the highest average posterior probability for the given input sample is selected. After obtaining a pixel-based crop classification map, a parcel-based procedure is applied to improve the quality and accuracy of the final map (Kussul et al., 2016). Crop type maps generated for 2013–2015 seasons are used to generate crop rotation violation map. By crop rotation violation, we mean growing the same crop type on the same field during at least 2 years in a row.

For 2016, when producing in season crop maps, we investigated availability of optical and SAR imagery to discriminate different crop type early in the season at acceptable target accuracy of 85%. In other words, in a situation of persistent cloud cover early in spring, can optical data be substituted with SAR imagery and whether the same level of performance can be achieved? In 2016, the test region experienced a lot of clouds during spring, so we considered the difference between using optical data from Sentinel-2 and SAR data from Sentinel-1A. Only one or two optical non-cloud images were available from March to June; at the same time we acquired 8 images from Sentinel-1A satellite (Table 1). For 2016 early season classification, we had three experiment designs: S1 – crop classification mapping using Sentinel-1A data only; S2 – using Sentinel-2 images only; and S1+S2 – crop classification mapping using combination of Sentinel-1A and Sentinel-2 images.

Performance metrics were estimated from ground validation datasets that were not used during classifiers training. The confusion matrix used in accuracy assessment provides information on the magnitude of the classification errors that allows an adjustment to be made in the area estimator (Olofsson, Foody, Stehman, & Woodcock, 2013). User's accuracy (UA)

and producer's accuracy (PA) are ways of representing individual class accuracy. User's accuracy means the probability that a pixel classified on the map represents the class on the ground whereas producer's accuracy indicates the probability of a reference pixel being correctly classified.

Results

Table 4 shows performance metrics for classification of satellite data for 2013–2015 seasons. We obtained reliable results with overall accuracy 85.3%, 90.1% and 92.4%, respectively, for 13 classes (Figure 3, Table A1-A3). Producer's (PA) and user's (UA) accuracies of winter wheat were always higher than 92%. Using only Landsat-8 optical data (2013–2014) winter rapeseed's PA and UA values were about 80% and 98%, respectively. When adding Sentinel-1 SAR data (2015), significant improvements were observed in detecting rapeseed (PA = 100%, UA = 94.6%). Also, fusion of SAR and optical data achieved gains of PA +15.4% and UA + 7% for sunflower. At the same time, addition of SAR data had no effect on detecting maize (PA and UA were approximately 90%), sugar beet (PA and UA were approximately 100%) and water (PA and UA were approximately 100%). Accuracy of soybeans (PA – 72.4%, 98.6% and 83.7%; UA – 80.8%, 87.3% and 78.9%) and spring and summer crops (PA – 25%, 76.4% and 66.7%; UA – 33.3%, 70.5% and 84.2%) varied widely from year to year.

Figure 4 shows a crop rotation violation map generated from single-year crop maps for 2013–2015. Winter wheat (with estimated total area of violations at 68,400 ha), winter rapeseed (5700 ha), sunflower (22,200 ha) and maize (85,800 ha) were grown at the same field at least twice during the past 3 years. It means that for these fields crop rotation requirements were not met.

Table 4. Comparison of producer accuracy (PA), user accuracy (UA) and overall accuracy (OA) for the Bilotserkivskiy district in 2013–2014 (based on Landsat-8) and 2015 (based on fusion Landsat-8 and Sentinel-1A).

| #	Class	2013		2014		2015	
		PA, %	UA, %	PA, %	UA, %	PA, %	UA, %
1	Artificial	100	100	72.4	28.3	-	-
2	Winter wheat	96	96	96.4	93.5	99.2	92.4
3	Winter rapeseed	83.3	100	80.5	98.1	100	94.6
4	Spring and summer crops	25	33.3	76.4	70.5	66.7	84.2
5	Maize	93	88.9	85.2	94.2	89.2	93.4
6	Sugar beet	100	100	97.2	99.9	100	100
7	Sunflower	80	75	84.6	87.5	100	94.5
8	Soybeans	72.4	80.8	98.6	87.3	83.7	78.9
9	Other cereals	75	63.2	1.2	5.6	-	-
10	Forest	87.5	100	98.6	95.6	99.7	99.9
11	Grassland	90.5	86.4	83.4	72.7	86.3	99
12	Bare land	80	100	100	87.2	100	95.9
13	Water	100	100	99.9	99.5	99.6	100
	OA, %	**85.6**		**90.1**		**92.4**	
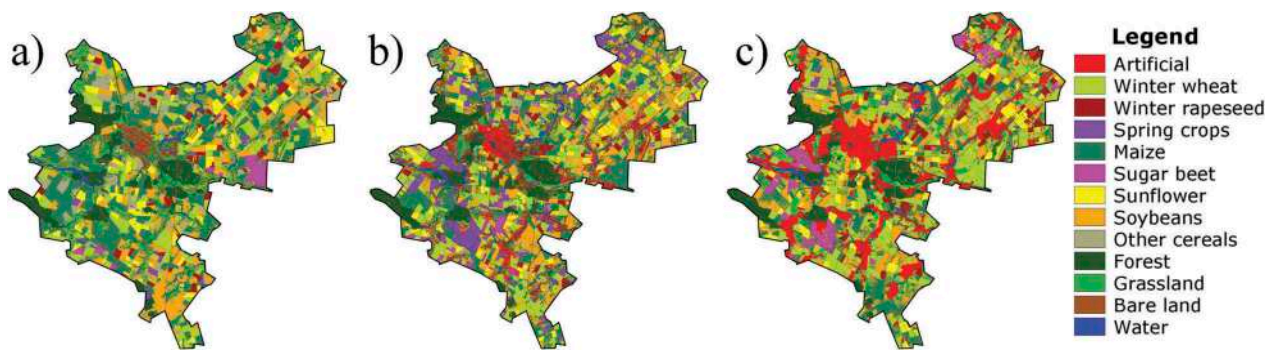
Figure 3. An example of classification results for Bilotserkivskiy district in 2013 (a), in 2014 (b), in 2015 (c).
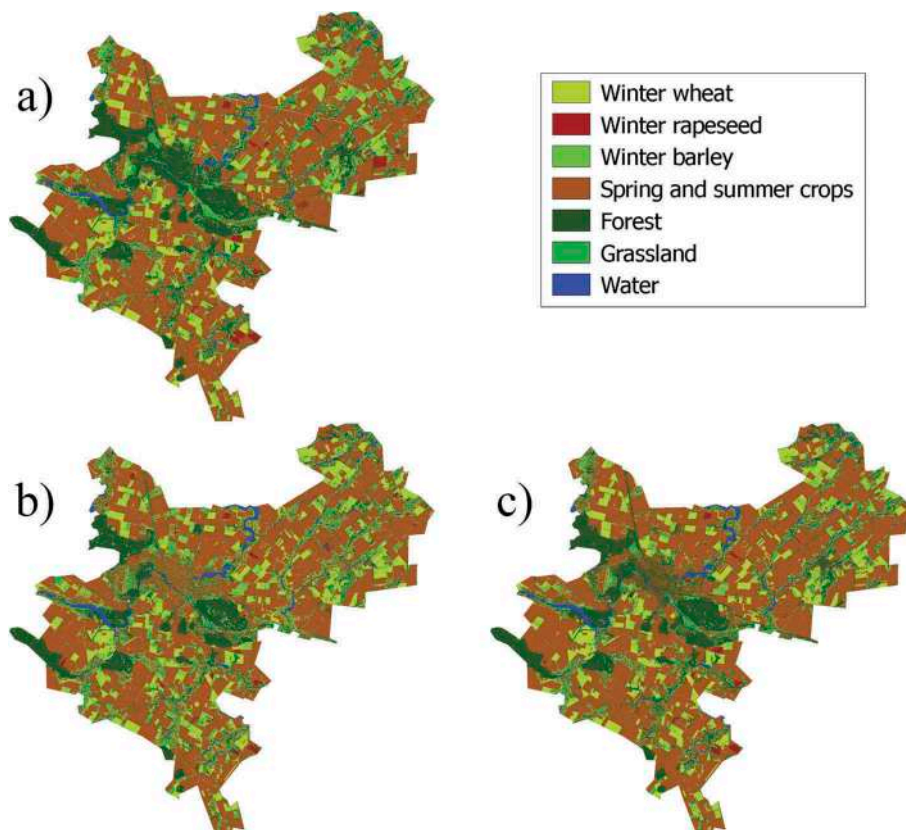
Figure 4. Crop rotation violation map for Bilotserkivskiy district based on crop classification maps in 2013–2015.

For 2016 early season classification, SAR data provided better results than optical due to the number of available images during the spring, when cloud cover was significant (Figure 5). Fusion of SAR and optical data allowed us to improve classification accuracy by +0.8% (Table 5). Winter rapeseed, spring and summer crops were discriminated with high accuracy (>85%). Winter wheat had higher user and producer accuracy. Unfortunately, reliable discrimination of winter barley and grassland is possible only in the end of the season.

Discussion and conclusions

This paper aimed at exploring the creation of yearly crop maps for the same region (Ukraine) utilizing different sets of available satellite imagery (both optical and SAR), and at different time periods (end of season and in season). This is the first such a study for Ukraine for producing multi-year crop type inventories, as previous studies focused on other regions (AAFC, 2013; Boryan et al., 2011; Johnson & Mueller, 2010), single year and end of season crop type maps only (Kussul et al., 2016; Prishchepov et al., 2012; Skakun et al., 2016b; Waldner et al., 2016). The proposed approach is very useful for operational crop mapping, as it can be applied, while satellite imagery being acquired and ingested into the classifier to provide both in season and end of season crop maps. Multi-year crop specific maps have multiple applications. One such application is detection of areas (fields), where crop rotation requirements (not to plant the same crop in consecutive years) were not met. Such maps are important

Figure 5. An example of classification result for Sentinel-1A images for Bilotserkivskiy district (a), Sentinel-2 time series for Bilotserkivskiy district (b), and fusion Sentinel-2 and Sentinel-1A images for Snigurivskiy district (c).
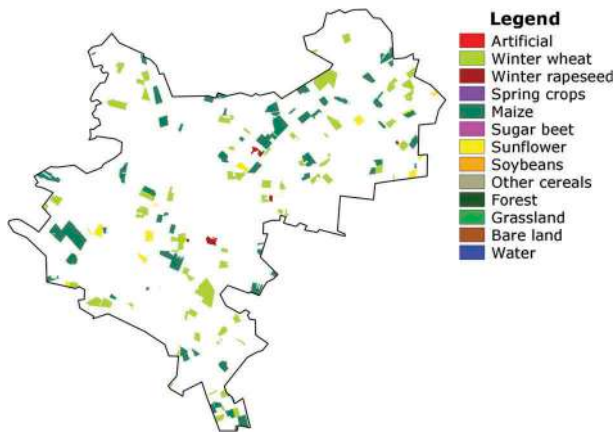
Table 5. Comparison of producer accuracy (PA), user accuracy (UA) and overall accuracy (OA) for the Bilotserkivskiy district in 2016 using Sentinel-1A and Sentinel-2 images.

		S1		S2		S1+S2	
	Class	PA, %	UA, %	PA, %	UA, %	PA, %	UA, %
1	Winter wheat	87.5	93	86.4	92.5	88	93.8
2	Winter barley	76.1	63.9	69	61.1	79.9	68.1
3	Winter rapeseed	96.4	91.6	90.9	59	97.2	91.8
4	Spring and summer crops	96.8	99.7	87.7	98.2	97.6	99.7
5	Forest	99.9	98.9	95.5	88.4	99.8	98.5
6	Grassland	61.5	25	84.3	23	66.8	29.8
7	Water	100	86	100	100	100	83.2
	OA, %	**92.9**		**87.3**		**93.7**	

for administrative authorities and government. It allows one to monitor compliance of crop rotation rules, which are necessary for preservation of soil degradation. In particular, violations of winter wheat, winter rapeseed, sunflower and maize were identified.

For early season classification, we provided comparison of crop classification maps based on optical data from Sentinel-2A and SAR data from Sentinel-1A (Table A4-A6). Due to considerable cloud cover, only two optical scenes were used for classification. While two optical scenes provided a decent performance achieving OA = 87.3%, the use of multi-temporal SAR images (8 scenes) outperformed the optical ones with OA = 92.9%. This was mainly because of larger number of SAR observations available comparing to the optical ones, and suggests that optical data can be substituted by SAR data early in season to discriminate winter crops, when cloud cover prevents getting optical data. This observation adds on to the results from Skakun et al. (2016b), which were mainly targeted of using SAR to better discriminate summer crops at the end of the agricultural season.

The derived yearly maps might find potential usage in the national cadaster system that is being developed in Ukraine at national level. Everyone could revise crop information for each parcel for previous years and detect corresponding crop rotation violations. The applications of the developed multi-year classification maps include stratification for ground surveys for crop area estimation and crop rotation violation area estimation, and providing crop-specific empirical crop yield forecasting models.

Disclosure statement

No potential conflict of interest was reported by the authors.

ORCID

Nataliia Kussul http://orcid.org/0000-0002-9704-9702
Lavreniuk Mykola http://orcid.org/0000-0003-2183-8833
Andrii Shelestov http://orcid.org/0000-0001-9256-4097
Sergii Skakun http://orcid.org/0000-0002-9039-0174

References

AAFC. (2013). ISO 19131 AAFC Annual crop inventory – data product specifications. Retrieved from http://www.agr.gc.ca/atlas/supportdocument_documentdesupport/aafcCropTypeMapping/en/ISO%2019131_AAFC_Annual_Crop_Inventory_Data_Product_Specifications.pdf

Becker-Reshef, I., Vermote, E., Lindeman, M., & Justice, C. (2010). A generalized regression-based model for forecasting winter wheat yields in Kansas and Ukraine using MODIS data. *Remote Sensing of Environment*, 114(6), 1312–1323.

Boryan, C., Yang, Z., Mueller, R., & Craig, M. (2011). Monitoring US agriculture: The US department of agriculture, national agricultural statistics service, cropland data layer program. *Geocarto International*, 26(5), 341–358.

Boryan, C.G., Yang, Z., Di, L., & Hunt, K. (2014). A new automatic stratification method for U.S. agricultural area sampling frame construction based on the cropland data layer. *IEEE Journal of Selected Topics in Applied Earth Observations and Remote Sensing*, 7(11), 4317–4327.

Cohen, W.B., & Goward, S.N. (2004). Landsat's role in ecological applications of remote sensing. *Bioscience*, 54(6), 535–545.

Franch, B., Vermote, E.F., Becker-Reshef, I., Claverie, M., Huang, J., Zhang, J., … Sobrino, J.A. (2015). Improving the timeliness of winter wheat production forecast in the United States of America, Ukraine and China using MODIS data and NCAR Growing Degree Day information. *Remote Sensing of Environment*, 161, 131–148.

Gallego, F.J. (2006). Review of the main remote sensing methods for crop area estimates, remote sensing support to crop yield forecast and area estimates. *ISPRS Archives*, XXXVI, 8/W48, 65–70.

Gallego, F.J., Kravchenko, O., Kussul, N., Skakun, S., Shelestov, A., & Grypych, Y. (2012). Efficiency assessment of different approaches to crop classification based on satellite and ground observations. *Journal of Automation and Information Sciences*, 44(5), 67–80.

Gallego, J., & Delincé, J. (2010). The European land use and cover area-frame statistical survey. In R. Benedetti,

M. Bee, G. Espa, F. Piersimoni, J. Wiley, L. Sons, & U.K. Chichester (Eds.), *Agricultural survey methods* (pp. 149–168). doi:10.1002/9780470665480.ch10

Johnson, D.M. (2016). A comprehensive assessment of the correlations between field crop yields and commonly used MODIS products. *International Journal of Applied Earth Observation and Geoinformation*, 52, 65–81.

Johnson, D.M., & Mueller, R. (2010). The 2009 cropland data layer. *Photogramm Engineering Remote Sensing*, 76, 1202–1205.

Kogan, F., Kussul, N., Adamenko, T., Skakun, S., Kravchenko, O., Kryvobok, O., … Lavrenyuk, A. (2013). Winter wheat yield forecasting in Ukraine based on earth observation, meteorological data and biophysical models. *International Journal of Applied Earth Observation and Geoinformation*, 23, 192–203.

Kuemmerle, T., Erb, K., Meyfroidt, P., Müller, D., Verburg, P. H., Estel, S., … Levers, C. (2013). Challenges and opportunities in mapping land use intensity globally. *Current Opinion in Environmental Sustainability*, 5(5), 484–493.

Kussul, N., Lavreniuk, M., Skakun, S., & Shelestov, A. (2017). Deep learning classification of land cover and crop types using remote sensing data. *IEEE Geoscience and Remote Sensing Letters*, 14(5), 778–782.

Kussul, N., Lemoine, G., Gallego, F.J., Skakun, S.V., Lavreniuk, M., & Shelestov, A.Y. (2016). Parcel-based crop classification in Ukraine using landsat-8 data and sentinel-1A data. *IEEE Journal of Selected Topics in Applied Earth Observations and Remote Sensing*, 9, 2500–2508.

Kussul, N., Skakun, S., Shelestov, A., Lavreniuk, M., Yailymov, B., & Kussul, O. (2015). Regional scale crop mapping using multi-temporal satellite imagery. *International Archives Photogramm Remote Sens Spatial Information Sciences*, XL-7/W3, 45–52.

López-Lozano, R., Duveiller, G., Seguini, L., Meroni, M., García-Condado, S., Hooker, J., … Baruth, B. (2015). Towards regional grain yield forecasting with 1km-resolution EO biophysical products: Strengths and limitations at pan-European level. *Agricultural and Forest Meteorology*, 206, 12–32.

Moreira, A., Prats-Iraola, P., Younis, M., Krieger, G., Hajnsek, I., & Papathanassiou, K.P. (2013). A tutorial on synthetic aperture radar. *IEEE Geoscience and Remote Sensing Magazine*, 1(1), 6–43.

Olofsson, P., Foody, G.M., Stehman, S.V., & Woodcock, C. E. (2013). Making better use of accuracy data in land change studies: Estimating accuracy and area and quantifying uncertainty using stratified estimation. *Remote Sensing of Environment*, 129, 122–131.

Pax-Lenney, M., & Woodcock, C.E. (1997). Monitoring agricultural lands in Egypt with multitemporal landsat TM imagery: How many images are needed? *Remote Sensing of Environment*, 59(3), 522–529.

Prishchepov, A.V., Radeloff, V.C., Dubinin, M., & Alcantara, C. (2012). The effect of Landsat ETM/ETM+ image acquisition dates on the detection of agricultural land abandonment in Eastern Europe. *Remote Sensing of Environment*, 126, 195–209.

Rahman, H., & Dedieu, G. (1994). SMAC: A simplified method for the atmospheric correction of satellite measurements in the solar spectrum. *International Journal of Remote Sensing*, 15(1), 123–143.

Shao, Y., Campbell, J.B., Taff, G.N., & Zheng, B. (2015). An analysis of cropland mask choice and ancillary data for annual corn yield forecasting using MODIS data. *International Journal of Applied Earth Observation and Geoinformation*, 38, 78–87.

Skakun, S., Kussul, N., Shelestov, A., & Kussul, O. (2016a). The use of satellite data for agriculture drought risk quantification in Ukraine. *Geomatics, Natural Hazards and Risk*, 7(3), 901–917.

Skakun, S., Kussul, N., Shelestov, A.Y., Lavreniuk, M., & Kussul, O. (2016b). Efficiency assessment of multi-temporal C-band Radarsat-2 intensity and Landsat-8 surface reflectance satellite imagery for crop classification in Ukraine. *IEEE Journal of Selected Topics in Applied Earth Observations and Remote Sensing*, 9, 3712–3719.

Skakun, S., Nasuro, E., Lavrenyuk, A., & Kussul, O. (2007). Analysis of applicability of neural networks for classification of satellite data. *Journal Autom Information Sciences*, 39(3), 37–50.

Song, X.P., Potapov, P.V., Krylov, A., King, L., Di Bella, C. M., Hudson, A., … Hansen, M.C. (2017). National-scale soybean mapping and area estimation in the United States using medium resolution satellite imagery and field survey. *Remote Sensing of Environment*, 190, 383–395.

Stefanski, J., Chaskovskyy, O., & Waske, B. (2014). Mapping and monitoring of land use changes in post-Soviet western Ukraine using remote sensing data. *Applied Geography*, 55, 155–164.

Taylor, J., Sannier, C., Delince, J., & Gallego, F.J. (1997). *Regional crop inventories in Europe assisted by remote sensing: 1988–1993* (Synthesis Report, EUR 17319 EN, JRC). Ispra.

Waldner, F., De Abelleyra, D., Verón, S.R., Zhang, M., Wu, B., Plotnikov, D., … Le Maire, G. (2016). Towards a set of agrosystem-specific cropland mapping methods to address the global cropland diversity. *International Journal of Remote Sensing*, 37(14), 3196–3231.

Table A1. Confusion matrix for 2013 when classifying multi-temporal Landsat-8 images.

Kappa = 0.82	1	2	3	4	5	6	7	8	9	10	11	12	13	UA
1	184	0	0	0	3	0	0	0	0	0	0	1	0	97.9
2	0	21,453	33	51	26	0	29	11	1728	0	2	30	0	91.8
3	0	1	3788	1	14	0	5	1	2	0	0	0	0	99.4
4	0	723	0	982	3	0	0	3	1101	0	24	0	0	34.6
5	0	0	0	177	33,972	2	390	4544	34	0	41	0	0	86.8
6	0	0	0	11	222	3511	118	52	2	0	2	0	0	89.6
7	0	1	0	10	389	7	13,241	1672	91	0	92	0	0	85.4
8	0	56	0	351	2660	181	1027	14,668	29	3	52	0	0	77.1
9	0	74	230	828	96	0	832	78	7677	0	24	0	0	78.0
10	0	27	0	0	78	0	36	11	6	4198	165	0	0	92.9
11	0	71	1	6	63	0	26	15	159	131	4089	31	0	89.0
12	0	0	0	0	0	0	0	0	0	0	4	403	0	99.0
13	0	0	0	0	0	0	49	0	0	0	0	0	2524	98.1
PA	100.0	95.7	93.5	40.6	90.5	94.9	84.1	69.7	70.9	96.9	91.0	86.7	100.0	85.3

Table A2. Confusion matrix for 2014 when classifying multi-temporal Landsat-8 images.

Kappa = 0.88	1	2	3	4	5	6	7	8	9	10	11	12	13	UA
1	210	12	23	0	139	2	31	4	90	68	163	0	0	28.3
2	10	36,984	0	518	22	0	0	42	1683	1	298	0	1	93.5
3	1	37	6608	0	0	90	0	0	0	0	3	0	0	98.1
4	0	240	1242	3693	45	0	0	1	0	0	19	0	0	70.5
5	0	440	200	163	16,902	0	35	174	33	0	4	0	0	94.2
6	0	3	2	0	0	6831	0	0	0	0	2	0	0	99.9
7	0	0	0	0	785	10	6702	1	9	0	156	0	0	87.5
8	0	343	2	74	1279	0	84	15,448	3	0	469	0	0	87.3
9	0	49	0	388	0	0	0	0	27	0	16	0	0	5.6
10	3	66	0	0	19	95	0	2	95	10,752	208	0	2	95.6
11	15	195	127	0	657	1	1074	3	393	79	6762	0	0	72.7
12	51	0	0	0	0	0	0	0	2	0	3	383	0	87.2
13	0	0	0	0	0	0	0	0	0	9	5	0	2880	99.5
PA	72.4	96.4	80.5	76.4	85.2	97.2	84.6	98.6	1.2	98.6	83.4	100	99.9	90.1

Table A3. Confusion matrix for 2015 when classifying multi-temporal Landsat-8 + Sentinel-1 images.

Kappa = 0.91	2	3	4	5	6	7	8	10	11	12	13	UA
2	9918	1	209	3	0	0	384	0	214	0	0	92.4
3	0	2177	78	0	0	0	46	0	0	0	0	94.6
4	0	0	576	38	0	0	67	0	3	0	0	84.2
5	0	0	0	17,918	0	0	1257	0	5	0	0	93.4
6	0	0	0	0	466	0	0	0	0	0	0	100
7	0	0	0	0	0	3191	184	0	3	0	0	94.5
8	73	0	0	2128	0	0	10,018	7	470	0	1	78.9
10	0	0	0	0	0	0	0	10,759	4	0	2	99.9
11	3	0	0	4	0	0	9	29	4433	0	1	99
12	0	0	0	0	0	0	0	0	2	301	11	95.9
13	0	0	0	0	0	0	0	0	1	0	3851	100
PA	99.2	100	66.7	89.2	100	100	83.7	99.7	86.3	100	99.6	92.4

Table A4. Confusion matrix for 2016 when classifying multi-temporal Sentinel-1A.

Kappa = 0.88	1	2	3	4	5	6	7	UA
1	29,711	965	8	1049	0	225	0	93
2	1479	3079	4	49	0	208	0	63.9
3	171	0	1875	1	0	0	0	91.6
4	94	0	11	60,229	0	100	0	99.7
5	28	0	45	1	6943	1	0	98.9
6	2485	3	3	851	10	1115	0	25
7	4	0	0	22	0	163	1159	86
PA	87.5	76.1	96.4	96.8	99.9	61.5	100	92.9

Table A5. Confusion matrix for 2016 when classifying multi-temporal Sentinel-2A.

Kappa = 0.81	1	2	3	4	5	6	7	UA
1	124,170	3218	482	5382	372	594	0	92.5
2	4176	7296	1	289	1	172	0	61.1
3	4764	0	7099	0	2	166	0	59
4	2832	0	61	174,228	10	370	0	98.2
5	2763	3	4	334	24,204	60	0	88.4
6	4955	63	159	18,410	758	7287	0	23
7	0	0	0	0	0	0	3727	100
PA	86.4	69	90.9	87.7	95.5	84.3	100	87.3

Table A6. Confusion matrix for 2016 when classifying multi-temporal Sentinel-1A and Sentinel-2A.

Kappa = 0.89	1	2	3	4	5	6	7	UA
1	29,902	813	5	1054	0	112	0	93.8
2	1233	3234	2	62	0	221	0	68.1
3	151	0	1891	17	0	0	0	91.8
4	87	0	7	60,713	4	81	0	99.7
5	68	0	36	4	6937	0	0	98.5
6	2521	0	5	315	12	1211	0	29.8
7	10	0	0	37	0	187	1159	83.2
PA	88	79.9	97.2	97.6	99.8	66.8	100	93.7